Available online at www.sciencedirect.com
SCIENCE DIRECT®
International Journal of Heat and Fluid Flow 24 (2003) 572–583
International Journal of HEAT AND FLUID FLOW
www.elsevier.com/locate/ijhff

Active cancellation of Tollmien–Schlichting instabilities on a wing using multi-channel sensor actuator systems

D. Sturzebecher *, W. Nitsche *

Technische Universität Berlin, Institut für Luft- und Raumfahrt, Sekr. F2, Marchstr. 12-14, 10587 Berlin, Germany

Received 25 November 2002; accepted 5 March 2003

Abstract

This paper describes investigations on active attenuation of naturally occurring Tollmien–Schlichting (TS) instabilities on an unswept wing. TS disturbances are canceled in their linear stage by superimposition with artificially generated counter waves in order to shift the laminar–turbulent transition downstream. In this method, the need for energy input is considerably lower than the stabilization by manipulation of the local mean velocity profile (e.g. boundary layer suction). An optimum TS wave cancellation is achieved by a fast digital signal processor performing an adaptive control algorithm. The oncoming traveling TS disturbances are detected by a reference sensor upstream of an actuator. The reference signal is directly calculated into an actuator signal by means of a linear transfer function. The transfer function is continuously adapted to minimize the error signal measured downstream of the actuator. Previous investigations with a single control system have shown the successful TS wave damping by an adaptive control algorithm. These investigations led to an improvement in the set up of sensors and actuators used in the field of TS wave control. As a follow up of these experiments, recent investigations focus on the application of multi-channel control systems. This approach is essential to attenuate three-dimensionally dominated boundary layer instabilities by spanwise arranged sensor–actuator systems. Furthermore, the employment of multiple sensor–actuator systems allows a streamwise repeated damping to extend the delay of laminar–turbulent transition considerably.

Keywords: Active wave control; Delay of laminar–turbulent transition; Sensor–actuator systems; Control of three-dimensional Tollmien–Schlichting instabilities; Streamwise repeated wave cancellation

1. Introduction

It is a well-known fact that the delay of laminar–turbulent transition leads to a significant reduction of skin friction. Many active and passive methods were investigated in this field. Most control techniques aim to stabilize the mean velocity profile of the boundary layer (e.g. boundary layer suction). The approach described in this paper deals with the cancellation of Tollmien–Schlichting (TS) instability waves by superimposing them with properly adjusted counter waves.

There are many known transition scenarios, but the transition in the 2D boundary layer of an unswept wing is dominated by TS instabilities. A typical TS dominated transition path can be described shortly as follows: outer perturbations (freestream turbulence and noise) are introduced at the leading edge and via the boundary layer (receptivity). The introduced disturbances are latent in the boundary layer and are amplified frequency-selectively starting from a critical chordwise Reynolds-number. The frequency range of these instabilities depends on the local stability of the mean velocity profile. In their first stage of development, the traveling harmonic instabilities are mainly two-dimensional. All existent TS modes grow independently, so that a linear superposition with artificially generated waves is possible without any destructive mode coupling. In their later stage, the development becomes more and more non-linear. Secondary instabilities lead to a heightened grow of three-dimensional disturbances. The three-dimensional distortion results in lambda vortices. The final transition is characterized by a decay of the lambda structures and succeeding,

* Corresponding authors. Tel.: +49-30-314-24449.
E-mail addresses: dirk.sturzebecher@web.de (D. Sturzebecher), wolfgang.nitsche@tu-berlin.de (W. Nitsche).

0142-727X/03/$ - see front matter © 2003 Elsevier Science Inc. All rights reserved.
doi:10.1016/S0142-727X(03)00051-1

randomly occurring, turbulent spots (e.g. Saric, 1992; Kachanov, 1994; Schlichting and Gersten, 2000).

Another type of instability dominates the transition scenario on swept wings. Due to the three-dimensional boundary layer, cross-flow (CF) instabilities are generated and amplified as stationary spanwise waves at the region of the leading edge. At smaller swept angles the CF disturbances are damped in the middle region of the wing chord and TS instabilities can cause the transition. But at higher swept angles, CF instabilities effect mainly the laminar–turbulent transition. Furthermore, the transition can also be triggered directly from leading edge disturbances (leading edge contamination, attachment line instabilities) at high swept angles (e.g. Bippes and Nitschke-Kowsky, 1987; Oertel and Delfs, 1996; Schlichting and Gersten, 2000).

However, TS disturbances are the main reason for laminar–turbulent transition on an unswept and on a moderate swept wing. Therefore, the attenuation of these harmonic perturbations effects an efficient delay of transition. The advantage of this technique is the much lower energy input compared with conventional methods of manipulating the mean velocity profile.

Many basic investigations have already proved the possibility of damping TS instabilities in their early linear stage by superimposition with anti-phase generated counter waves (e.g. Milling, 1981; Liepmann et al., 1982). These experiments were conducted primarily using artificial mono-frequent disturbances, which were superimposed by the same disturbance with a properly adjusted amplitude and phase shift. Some other works in this field have dealt with the problems surrounding the random occurrence of broad-band natural TS wave packets (e.g. Thomas, 1983). Ladd and Hendricks (1988) reported the application of a digital transfer function continuously adapted by a gradient descent algorithm to attenuate 2D TS instabilities on an axisymmetric body in a water tunnel. Subsequent studies on the same test body (Ladd, 1990) describe the use of a classical control system consisting of a reference sensor, an actuator and an error sensor. This set up enabled a reduction of the wall shear stress fluctuation of around 50%. Pupator and Saric (1989) involved transfer functions based on the fast Fourier transformation to calculate appropriate counter disturbances. More recently, the work of Herbert et al. (1996) reports the application of a neural network on a basic control unit to attenuate TS disturbances successfully.

A large number of numerical investigations in the field of active TS wave cancellation were implemented. Joslin et al. (1995) conducted direct numerical simulations to attenuate TS waves with a sensor–actuator arrangement on a flat plate. The spectral control approach applied was essentially aimed at the direct conversion of a sensor signal measured upstream into an actuating signal by adapting amplification and phase shift. The work of Gmelin et al. (2000), to quote yet another example, describes the use of several control techniques leading to a successful damping of linear and also non-linear TS waves. These investigations have shown that the use of digital linear filters (FIR filter, finite impulse response) seems to be the most promising method of yielding a high reduction of linear TS instabilities. The concepts of the non-linear methods are aimed primarily at reducing the resonant behaviour of 2D and 3D instability modes.

Natural TS instabilities occur randomly as wave packets. Therefore, an effective damping can be obtained only by a closed loop feed-forward control algorithm working in real time. An adaptive linear control algorithm performed by a fast signal processor is applied successfully for cancelling natural TS instabilities on an unswept wing at TU-Berlin for several years (e.g. Baumann and Nitsche, 1996, 1997; Baumann et al., 2000). The principle of this approach is shown in Fig. 1(a). The traveling TS waves are measured by a sensor upstream of an actuator. The actuator signal is derived from the reference signal via a transfer function. This transfer function is continuously adapted in order to minimize the error signal measured downstream of the actuator. Characteristic sensor and actuator signals with control (AWC) and without control are depicted in Fig. 1(b).

Unfortunately, a complete damping of all TS instabilities is not possible. The remaining disturbances are amplified again and also lead to transition. Therefore, the wave attenuation is repeated in streamwise direction to detect and cancel the remaining perturbations in order to extend the delay in transition considerably. In

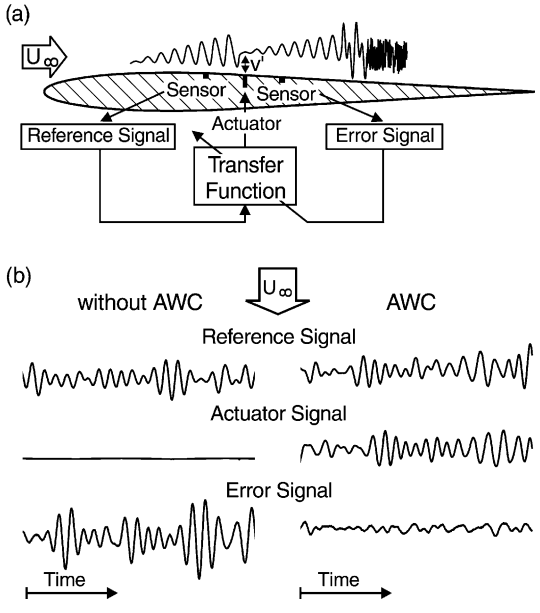

Fig. 1. (a) Principle of active TS wave control (AWC) and (b) typical sensor and actuator signals with and without control.

addition, TS waves can vary in phase and amplitude in spanwise direction caused by three-dimensional instability waves as well as a spanwise independent formation of TS perturbations. For this reason, recent investigations concentrate on multiple application of sensor–actuator systems in spanwise as well as streamwise arrangements (Sturzebecher and Nitsche, 2002; Sturzebecher, 2002).

2. Experimental set up

Investigations on active TS cancellation were carried out on an unswept test wing at a freestream velocity of $U_\infty = 17$ m/s. The symmetric airfoil used has a modified NACA 0008 profile and a main chord length of $c = 1.3$ m. The test wing has an interchangeable wing segment ($x/c = 0.39$–0.78), which allows the integration of different sensor–actuator arrangements depending of the experimental application. A 3D source was installed at $x/c = 0.3$ to generate artificial 2D waves as well as 3D disturbances, such as oblique waves or point-source induced instabilities in addition to the investigations on natural TS instabilities. The 3D source consists of spanwise arranged small wall-bounded slots ($\Delta z = 7$ mm), which are capable of introducing phase shifted perturbations.

2.1. Sensor / actuator

An accurate damping of TS instabilities requires highly sensitive sensors, which are able to detect tiny TS waves in their early linear stage. From this point of view, the most conventional sensor techniques (e.g. surface hot film, microphone) are not satisfactory. For this reason, the surface hot wire was designed especially for experiments on active wave control (e.g. Sturzebecher et al., 2001). A platinum-coated tungsten wire ($\phi = 5$ μm) is welded over a narrow cavity (0.075–0.1 mm) flush to the wing surface (Fig. 2). The heat flux into the wall can be considerably reduced by this arrangement of the hot element. This leads to a signal to noise ratio improved by five times compared with a conventional surface hot film. Flexible circuit boards with a 30–75 μm copper layer are usually employed to manufacture arrays of surface hot wires. The cavity is grooved in the copper layer using the photo-etching technique. Low-speed experiments have shown that the surface roughness effect of the sensor's cavity is negligible.

A flush-mounted actuator is needed to introduce anti-waves. The spanwise resolution with single actuators should be sufficient to approximate the spanwise wavelength of the 3D waves to be damped. The slot actuator is the most preferable actuating device, because of its simple set up. Fig. 3(a) shows a basic sketch of this type

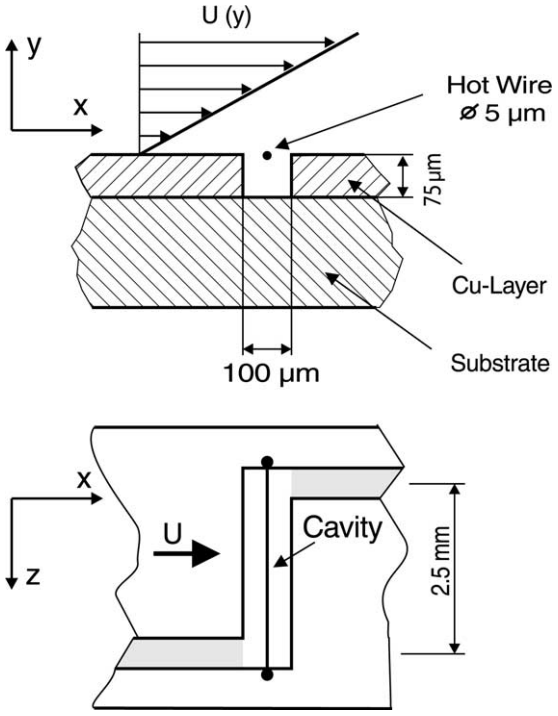

Fig. 2. Surface hot wire.

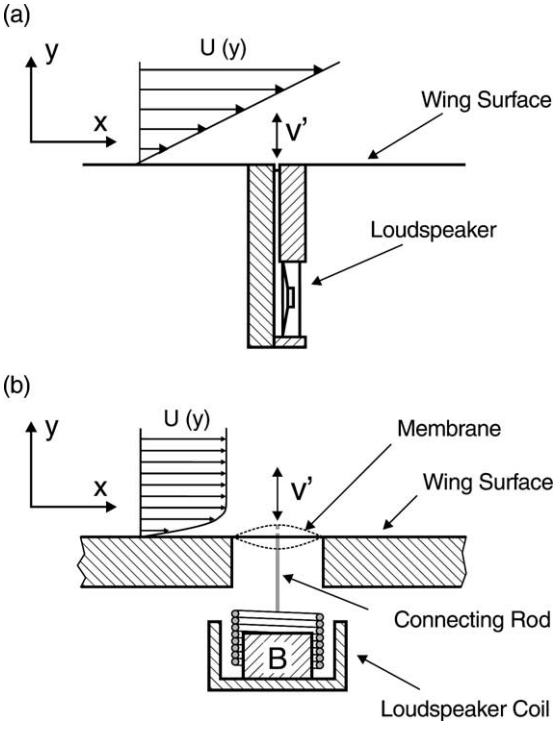

Fig. 3. (a) Slot actuator and (b) membrane actuator.

of actuator. Loudspeakers arranged spanwise underneath a small wall-bounded slot ($t = 0.2$ mm) induce an oscillating fluctuation perpendicular to the wing surface by vibrating the loudspeaker diaphragms. Separating walls between the autonomously operated loudspeakers

enable the slot actuator to introduce 3D waves into the boundary layer. These narrow walls end a few millimeters below the wing surface to obtain a smooth phase shift between the individually controlled single actuators.

Another actuating principle employed is the membrane actuator (Fig. 3(b)). A flush-mounted membrane is driven by a powerful solenoid via a T-shaped connecting rod. A highly elastic membrane material was chosen to allow sufficient wall displacement with relatively short membrane length in streamwise direction. It is possible to manufacture membrane length of approximately one quarter of a TS wavelength ($t = 6$ mm). Three-dimensional anti-waves are generated by spanwise arranged solenoids and connecting rods driving a common membrane. As shown in Section 3, the achievable local damping can be considerably improved using a membrane rather than a slot actuator. This is attributable to the smoothed introduction of counter waves and the flush set up by the closed surface.

2.2. Adaptive control

The method of active wave control (AWC) is a derivation of a control algorithm initially applied in the field of active noise control (e.g. Elliott and Nelson, 1993). A finite impulse response (FIR) filter is used as an internal transfer function to adapt the amplification and the propagation of TS waves in their linear stage. FIR filters are qualified for accurately modeling the development of TS instabilities in the boundary layer.

FIR filters represent in principle the system response to an impulse. Eq. (1) describes the mathematical formulation of the continuous convolution between the FIR filter and the input signal. The nth output sample $y(n)$ is calculated by the dot product of M filter coefficients $h_0 - h_{M-1}$ and M preceding samples of the input signal $x(n) - x(n - M + 1)$

$$y(n) = \sum_{i=0}^{M-1} h_i \cdot x(n-i) \tag{1}$$

Additionally, the flow chart in Fig. 4 describes the procedure of convolution graphically. In other words, the convolution performed continuously is a weighted moving average of M past inputs. The application of a FIR filter effects only a change of the output signal. Therefore, these filters are characterized as non-recursive.

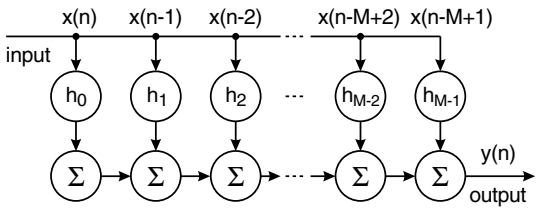

Fig. 4. FIR filter.

Fig. 5 depicts the flow graph of the algorithm applied. A reference sensor upstream of the actuator detects the traveling TS disturbances (x). The actuator signal (y) is, as already defined above, the result of the continuously sliding calculated dot product between the primary FIR filter (FIR A) and the reference signal (x). The primary transfer function is permanently adapted in order to minimize the error signal (e), measured downstream of the actuator. The path between actuator and error sensor is pre-adapted beforehand with a system identification algorithm.

This error path (FIR C) emulates the time delay of the wave superposition, the actuator and the error sensor. The weight taps of the primary FIR filter (FIR A) are continuously adapted following the steepest descent of the square error signal (e^2). The gradient method used for the filter update is based on the least-mean-square (LMS) algorithm. This means that, each filter coefficient is modified by adding a small percentage (μ^*) of the negative gradient of the quadratic error function $e^2(n) = f(h_i)$ to update the filter weights in such a manner that the error signal is minimized (Eq. (2)) (e.g. Snyder, 2000)

$$h_i(n+1) = h_i(n) - \mu^* \cdot \frac{\partial e^2(n)}{\partial h_i} \tag{2}$$

The gradient of the quadratic error signal can be deduced very simple by calculating the difference between desired and estimated output signal $e^2(n) = (d(n) - y(n))^2$ (Eq. (3)). The estimated output is determined by Eq. (1), whereas the FIR filter models a transfer function of the path to be identified (e.g. Wirnitzer et al., 1994; Elliott, 2001)

$$\frac{\partial e^2(n)}{\partial h_i} = -2 \cdot e(n) \cdot x(n-i) \tag{3}$$

The "filtered-x-LMS" procedure considers the error path to get a filtered reference signal (y_2). A correlated error signal (r) is derived from the filtered reference and

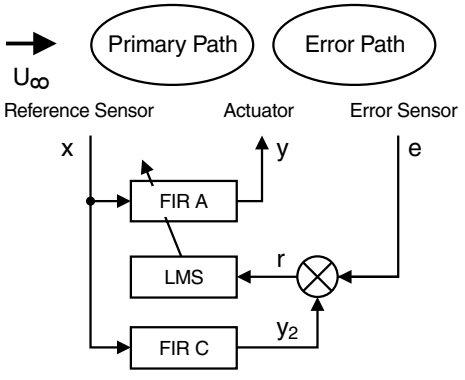

Fig. 5. Filtered-x-LMS algorithm (single).

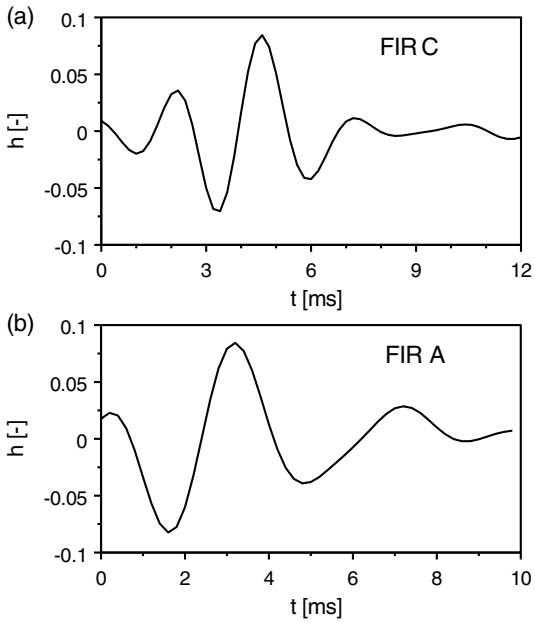

Fig. 6. (a) FIR model of error path (FIR C) and (b) FIR model of primary path (FIR A).

the error signal, which is applied to perform the LMS algorithm. Therefore, the LMS update of the filter coefficients with respect to the Eqs. (2) and (3) can be formulated as follows in Eq. (4), whereas $\mu = 2\mu^*$ terms the convergence coefficient

$$h_i(n+1) = h_i(n) + \mu \cdot e(n) \cdot y_2(n-i) \tag{4}$$

Typical adapted FIR filters causally modeling the error path (FIR C) and the primary path (FIR A) are illustrated in Fig. 6(a) and (b). The waviness of the filters shows the characteristic of a band-pass filter expressing the frequency-selective amplification of the TS waves. Furthermore, the delay of the wavy pulse is the modeled convection time of the TS disturbances.

A digital signal processor system (SHARC, ADSP-21060) extended by an interface has direct access to a 16-channel A/D converter and a 16-channel D/A converter. The floating-point processor has a performance of 60 MFLOPS. Usually, sampling rates of 5 kHz and filters with 30–80 coefficients are employed for an effective TS wave cancellation. Due to the A/D and D/A interface, the processor can control up to eight sensor–actuator systems simultaneously by adapting autonomous as well as coupled transfer functions. The programming is based on an assembler language. Some basic macros enabling a time-optimized processor programming, e.g. an optimized macro for the calculation of the dot product, are available (Smith, 1998) and were implemented to apply multi-channel filtered-x-LMS algorithms.

3. Actuator investigations

In addition to the sensors and the control algorithm, the choice of actuators is one of the most important aspects in the field of active TS wave cancellation. The actuator must be able to generate waves corresponding to the characteristic frequencies and wavelengths of TS instabilities. The response of the actuator should be linear with a time delay that is smaller than the convection time of the TS waves between reference sensor and actuator. As already mentioned, the slot actuator is usually preferred because of its simple set up. However, the slot acts as a surface roughness element causing additional disturbances especially at higher Reynolds numbers. Furthermore, non-linear effects in inducing TS waves around the slot degrade the local damping. Obviously, flush-mounted membrane actuators have a much better behavior than slot actuators. Comparative investigations were carried out to emphasize this

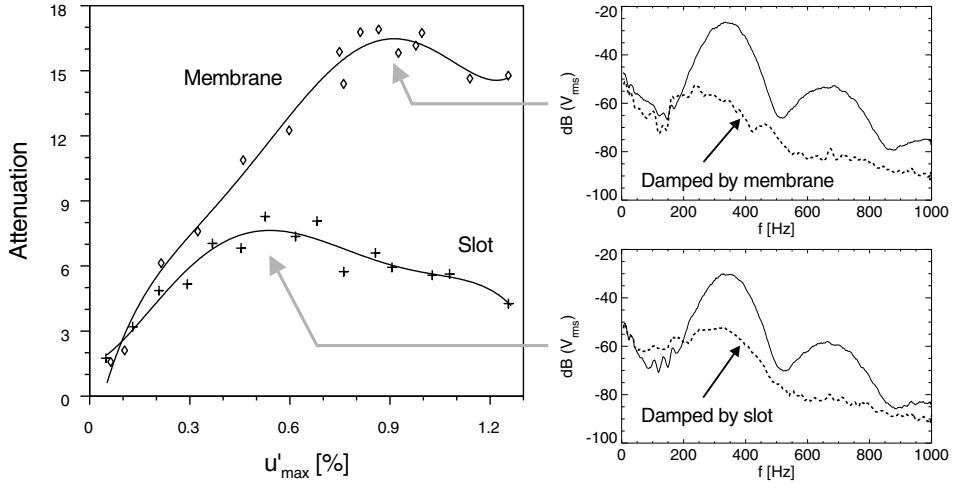

Fig. 7. Achievable attenuation of slot and membrane actuator.

assumption. Both actuator principles were applied as a 2D actuator driven by spanwise averaged reference and error signals in a single control system (Sturzebecher and Nitsche, 2002).

Fig. 7 shows the attenuation achieved by both actuators expressing the ratio between the root-mean-square (RMS) values of the error signal measured in uncontrolled and controlled case. The attenuation is plotted versus the maximum velocity fluctuation (u'_{max}) measured at the actuator position. The local disturbance was induced by the above-mentioned 3D source introducing a random-noise excited 2D wave with varying amplitudes. The membrane actuator is capable of reducing the local disturbance by factor 16 at $u'_{max} \approx 0.9\%$. The slot actuator achieves an optimum reduction of about *eight* at $u'_{max} \approx 0.5\%$, whereas the membrane actuator obtains a damping factor of 10 at the same disturbance amplitude. Obviously, the membrane actuator is more suitable for generating accurate counter waves. Moreover, the depicted power spectra of the error signal shown for the optimum reduction case of both actuators also confirm the superiority of the membrane (Fig. 7).

4. Control of three-dimensional instabilities

An appropriate spanwise arrangement of sensors and actuators is required to detect and cancel three-dimensional TS waves. These spanwise arranged single control systems are operated by individually adapted transfer functions (Fig. 8). The results described were obtained by a multi-channel control consisting of eight spanwise arranged sensor–actuator systems. The 3D membrane actuator used was spanwise separated into eight individual actuators with a span of $\Delta z = 14$ mm. The two outer actuators have twice the span ($\Delta z = 28$ mm) in order to reduce the interaction with the uncontrolled flow. An eight-sensor array located approximately 1.5 TS wavelengths upstream of the actuator ($\Delta x = 32.5$ mm) delivers the reference signals. The lateral spacing corresponds with the single actuator span. A 16-sensor array positioned approximately 3 TS wavelength downstream of the actuator ($\Delta x = 62.5$ mm) has a spanwise spacing of $\Delta z = 7$ mm. Every second sensor of this array is used as an error sensor corresponding with the above-mentioned lateral spacing. The set up described ensures optimum control of TS waves with oblique angles of $\psi \leqslant 16°$.

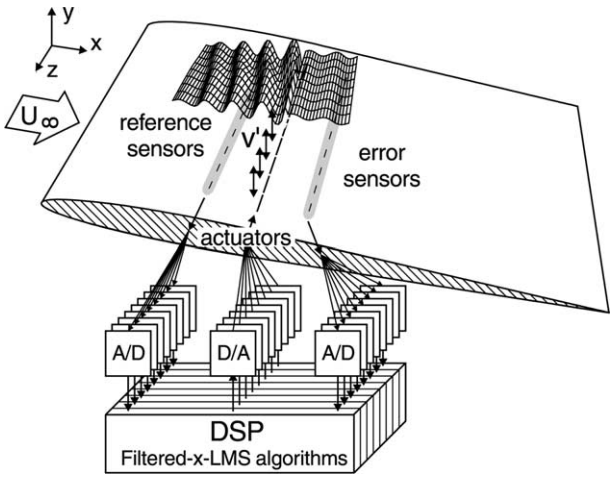

Fig. 8. Principle of 3D control.

Fig. 9(a) depicts the time traces of the 16 error sensors when natural perturbations occur. Typical TS wave packets are simultaneously recognizable in all 16 signals. This shows that naturally occurring TS instabilities at the unswept test wing are predominantly two-dimensional. The disturbances at the edge of the error array show a slightly increased amplitude. This indicates three-dimensional parts which amount to approximately 10% in the TS perturbations. A considerable damping of natural TS instabilities can be observed if the control is activated (Fig. 9(b)). A significant reduction in all 16 error signals is obtained even though only every second sensor serves as error input for the control. The remaining disturbances are obviously random but very small.

The spanwise 16-error-sensor array ensures a spatial time-resolved data acquisition. This data set can be transformed into the frequency and the spanwise wavenumber domain using the Fourier analysis. Fig. 10(a) depicts the frequency–wavenumber spectrum for slightly amplified natural TS disturbances corresponding with the time traces shown above (Fig. 9(a)). The wavenumber k_z represents the inverse spanwise wavelength normalized by twice the span of a single sensor–actuator system (2×14 mm). A value of *one* denotes the Nyquist wavenumber of the spanwise arranged sensor–actuator systems which corresponds with a spanwise wavelength of 28 mm. The wavenumber $k_z = 0$ characterizes the pure 2D wave. The wavenumber axis ranges up to *two*, due to the double resolution of the error-sensor array ($\Delta z = 7$ mm). Evidently, 2D disturbances prevail in the natural TS structure on the test wing. This is clearly indicated by a maximum at wavenumber $k_z = 0$ in the TS instability domain (200–400 Hz), as well as by a sub-maximum, also at $k_z = 0$, in the domain of higher harmonic TS frequencies (550–750 Hz). Three-dimensional disturbances are also recognizable in both of these frequency ranges, but the amplitude of these coefficients decreases at higher spanwise wavenumbers. Fig. 10(b) shows the frequency–wavenumber spectrum of the error-sensor array at activated wave cancellation. An attenuation of about 28 dB (reduction by ≈94%) can be observed in the domain of maximum TS disturbances ($f = 200$–400 Hz, $k_z \leqslant 0.2$). A high reduction is also attained in the three-dimensional domain within the

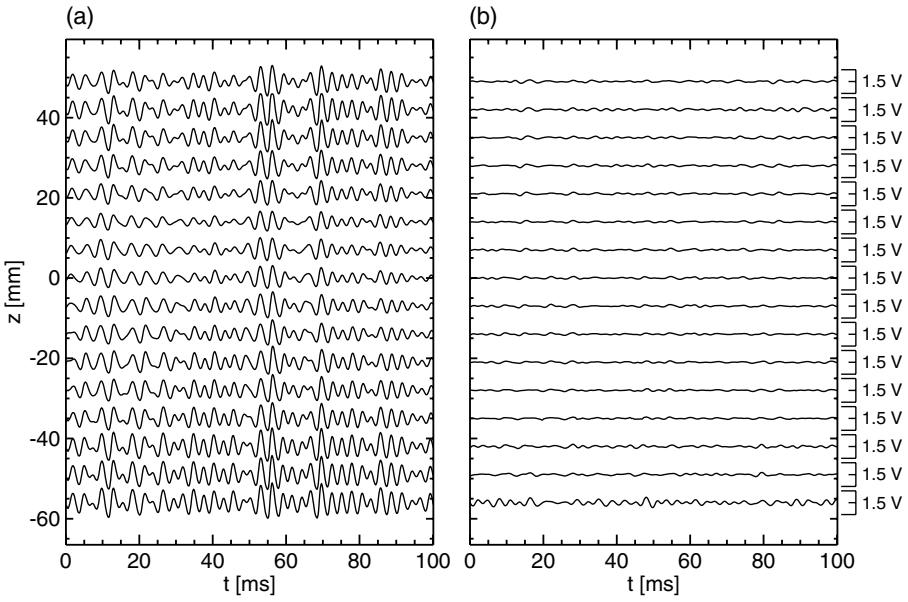

Fig. 9. Error-sensor signals at natural disturbances: (a) without and (b) with 3D control.

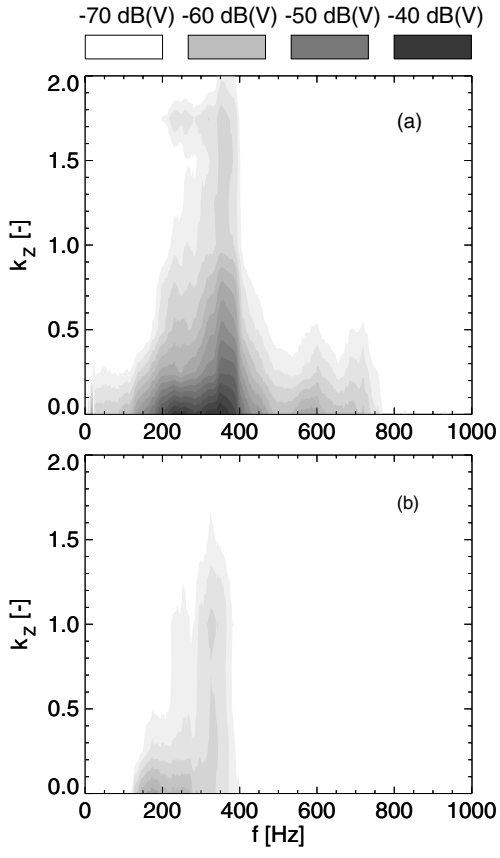

Fig. 10. Frequency–wavenumber spectra of the error-sensor array at natural disturbances: (a) without and (b) with 3D control.

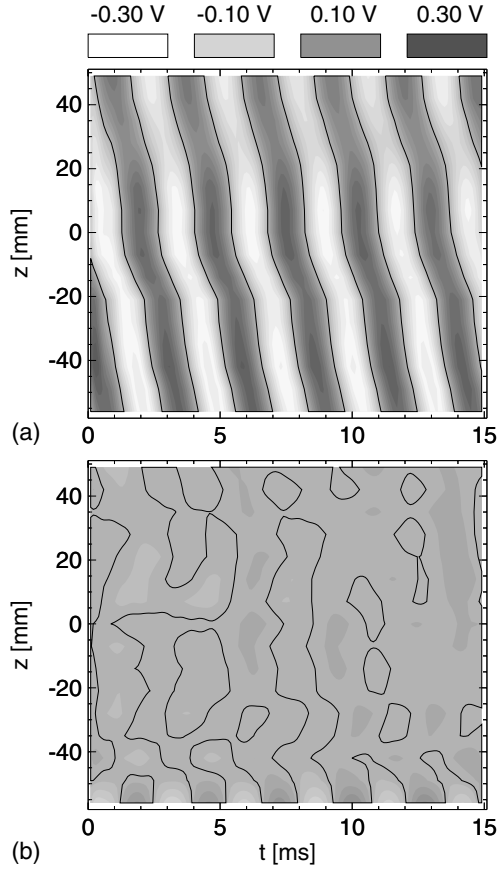

Fig. 11. Contour plot of error-sensor time traces in case of oblique TS wave: (a) without and (b) with 3D control.

fundamental TS frequencies. Experiments indicate that not less than five spanwise arranged single actuators are required to attain a sufficient approximation of a complete spanwise wavelength. The reduction of TS waves above $k_z > 0.5$ ($\lambda_z < 56$ mm) is therefore not a result of

3D damping. In fact, it is the direct consequence of the mode coupling with the attenuated fundamental instabilities.

As already mentioned, naturally occurring TS waves at the test wing are two-dimensionally dominated. From this point of view, it was essential to verify the reliability of the multiple spanwise control system by means of artificially generated three-dimensional TS waves. These 3D waves were introduced into the boundary layer by a slot source located upstream ($x/c = 0.3$) consisting of spanwise arranged small slots, which operate phase-shifted. Fig. 11(a) represents the contour plot of the error-sensor time traces at an artificially induced wave with a frequency of $f \approx 350$ Hz. The adjusted spanwise wavelength of $\lambda_z \approx 110$ mm is equivalent to an oblique traveling angle of $\Psi \approx 10°$. A considerable damping of this three-dimensional TS wave is made possible due to the spanwise arrangement of sensors and actuators (Fig. 11(b)). The minor disturbances remaining have obviously no regular structure.

The spanwise measured error time traces (Fig. 11(a)) enable the Fourier transformation into the frequency and wavenumber domain to assess the modal composition of the TS disturbances. The frequency–wavenumber spectrum derived is shown in Fig. 12(a). A significant maximum is recognizable at $f \approx 350$ Hz and $k_z = 0.25$. This spanwise wavenumber denotes a spanwise wavelength of $\lambda_z = 112$ mm. In addition, a sub-maximum can be identified at twice that of the fundamental frequency between the harmonic and second harmonic wavenumber ($f \approx 700$ Hz, $k_z = 0.25$–0.5). This sub-maximum is caused by coupling with the fundamental instability modes. A significant attenuation of the fundamental 3D mode as well as the higher harmonic mode can be observed in case of activated control (Fig. 12(b)).

The multiple spanwise control system was additionally investigated with point-source induced TS instabilities. Only one single chamber ($b = 7$ mm) of the slot source was driven by sinusoidal disturbances ($f = 300$ Hz). This form of excitation causes a curve-shaped wave pattern as illustrated in the contour plot of the error signals (Fig. 13(a)). The corresponding spatial wave can be imagined as 180° view rotated. An oblique angle continuously changing in spanwise direction, caused by the spanwise dispersed development, can be observed. It follows that numerous 3D instability modes are present. A significant attenuation of this multi-modal disturbance is also achieved by using a multiple spanwise control system (Fig. 13(b)).

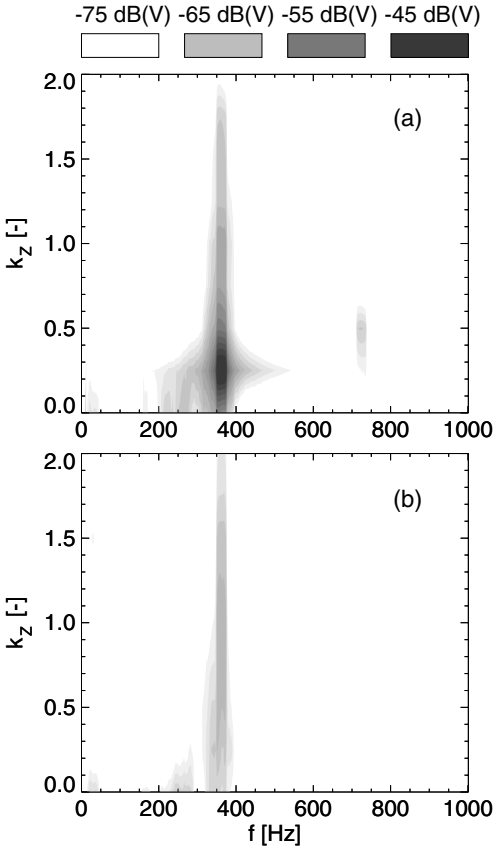

Fig. 12. Frequency–wavenumber spectra of the error-sensor array in case of oblique TS wave: (a) without and (b) with 3D control.

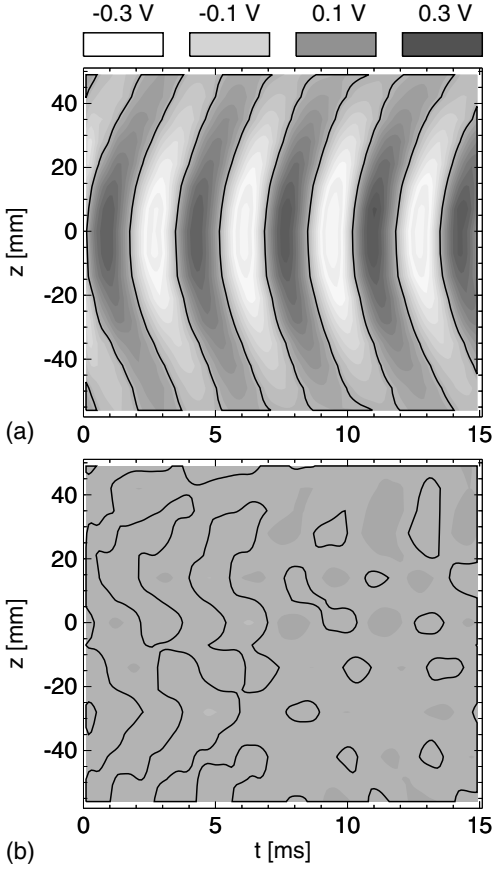

Fig. 13. Contour plot of the error signals at point-induced TS instabilities: (a) without and (b) with 3D control.

The transformation of these error signals into the frequency and wavenumber domain delivers the modal composition of the point-source induced disturbance with and without damping (Fig. 14). The spectrum of the uncontrolled case (a) documents, as already outlined above, the multi-modal character of the perturbation structure. The Fourier approximation of the continuously changing oblique angle in spanwise direction needs a broad weighting of the coefficients in the wavenumber domain. In fact, the coefficients at $f = 300$ Hz are raised in the range of $k_z = 0$–0.5. Furthermore, higher harmonic partitions appear at $f = 600$ Hz in a similar wavenumber range as the fundamental disturbance. A strong damping of these modes can be recognized at activated control (Fig. 14(b)). It is evident, that in this disturbance case, too, modes above wavenumber $k_z = 0.5$ are damped even though an appropriate spanwise generated wavelength requires more than five actuators ($k_z \leqslant 0.5$).

Experiments with artificially generated instabilities have proved that the spanwise distribution of sensors and actuators is sufficient to obtain an optimum damping of all instability modes on the unswept test wing. Further investigations have shown that a spanwise coupling of adjacent single systems via additional transfer functions is not necessary. No further advanced attenuation could be detected even though the adapted coupling transfer functions were causal. Hence, it is preferable to keep the time exposure low by using autonomous transfer functions. However, future signal processors will not be limited to modeling an increased number of transfer functions. This could make spanwise control systems feasible, which provide the same damping effect but require fewer sensors and actuators than uncoupled systems. Moreover, a spanwise coupling compensation is capable of improving the wave cancellation under 3D flow conditions (e.g. spanwise pressure gradient).

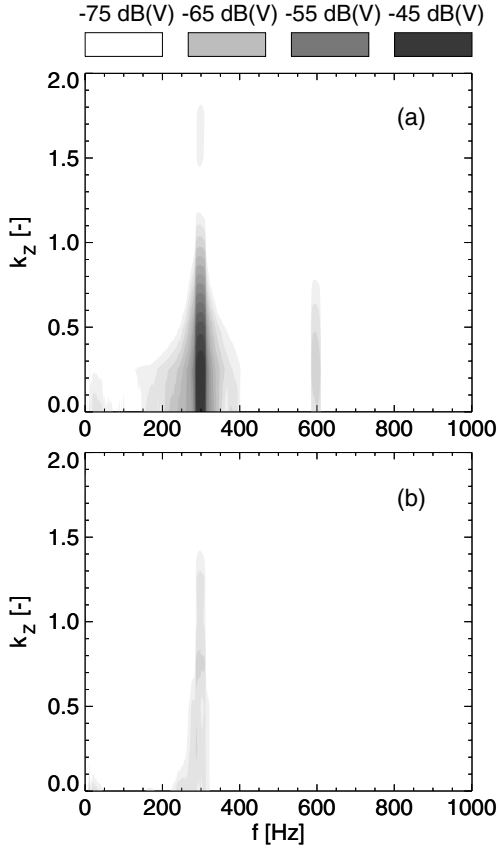

Fig. 14. Frequency–wavenumber spectra (error sensor array) at point-source induced instabilities: (a) without and (b) with 3D control.

5. Streamwise repeated control

There are many reasons that inhibit a complete cancellation of TS instabilities. Analog and digital noises constrict the detection of very small TS disturbances as well as the generation of small counter waves. Furthermore, a weak non-linear TS development degrades the efficiency of the linear control approach. The transition delay attained by a single-stage attenuation can be very small especially under conditions of a high adverse pressure gradient. A streamwise repeated control is therefore essential to yield a profitably extended delay of the laminar–turbulent transition at the wing of an aircraft.

The principle of repeated control as well as the set up used are shown in Fig. 15. Three slot actuators were positioned with a distance of about four TS wavelength ($\Delta x = 80$ mm) between two streamwise actuators. Four spanwise sensor arrays served as reference and/or error sensors. These arrays were located between the actuators, as well as upstream of the first and downstream of

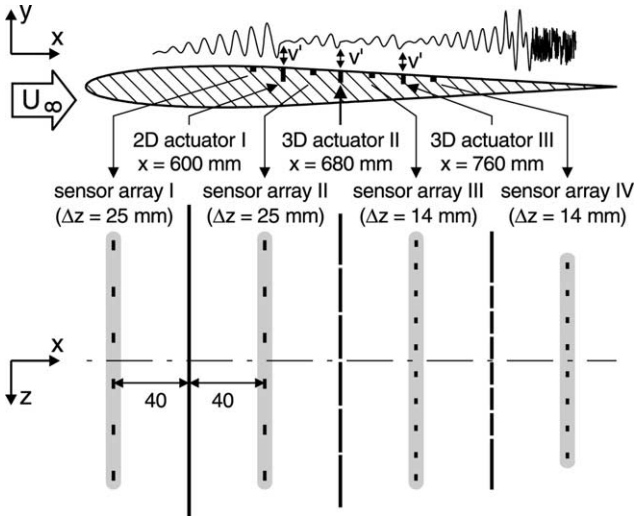

Fig. 15. Streamwise repeated TS wave control.

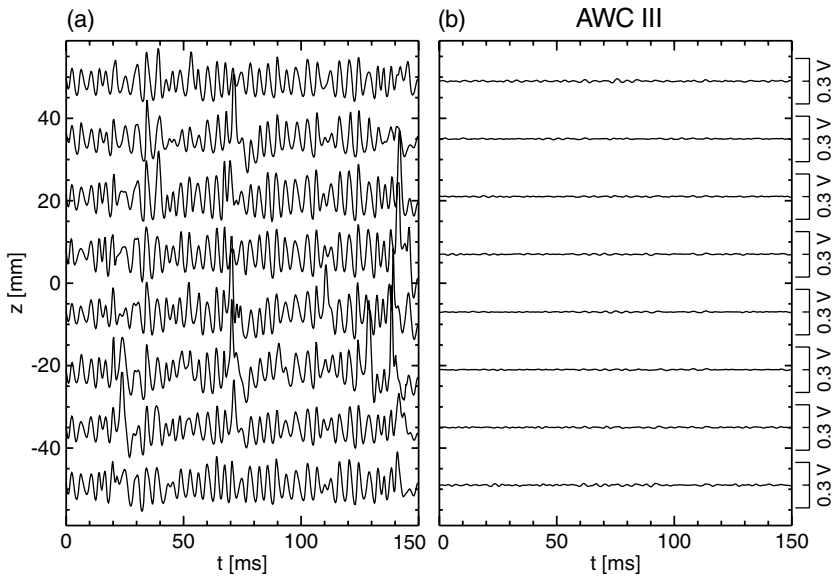

Fig. 16. Time traces of sensor array IV: (a) without control and (b) all control systems activated (AWC III).

the last actuator. The first actuator was designed to cancel 2D waves only. The second actuator was separated into a six-chamber actuator with a $\Delta z = 25$ mm to damp the growing share of 3D modes. The following third actuator consists of eight single slot actuators with a span of $\Delta z = 14$ mm each. The respective sensor arrangements were suitable for this spanwise resolution.

The adaptation of all control systems commenced successively in streamwise direction. The control systems following downstream were not activated until the preceding system had achieved a sufficient cancellation. The local damping effect of the streamwise repeated TS wave control is shown by the time traces of the sensor array IV. The signals indicate the strong non-linear stage of TS development at this position without control (Fig. 16(a)). The time traces contain single non-linear spikes, which characterize the onset of turbulent events. A linear control approach would fail under this condition. A very intense local damping can be observed when all three control cascades are activated (Fig. 16(b)).

Fig. 17(a) depicts the spanwise distribution of the RMS values delivered by sensor array IV with successively employed control cascades and without damping. The uneven spanwise RMS value distribution in the uncontrolled case is caused by the occurrence of strong non-linear events mentioned above. The stepwise applied control stages obtain a corresponding spanwise smoothed reduction of the disturbance intensity gathered at sensor array IV. The spanwise averaged time traces of this sensor array deliver a 2D spectrum for each control case (Fig. 17(b)). The sporadic occurrence of non-linear events in the uncontrolled case effects broad-band increased Fourier coefficients. The activation of the first cascade already delivers a broad-band

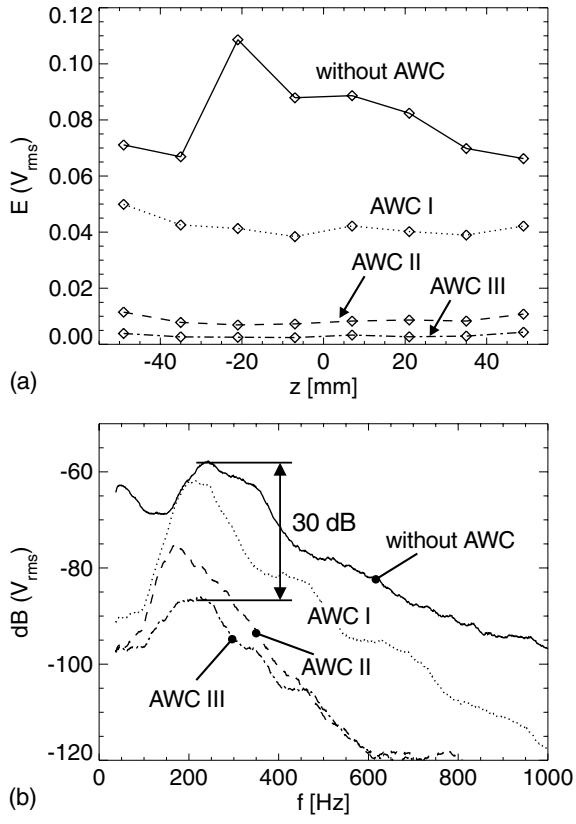

Fig. 17. (a) RMS distribution and (b) 2D spectra at the sensor array IV.

damping of the spectrum. The linear damping of TS instabilities further upstream causes a suppression of the non-linear spikes at the depicted sensor position. A substantial TS reduction can be observed, if the first two

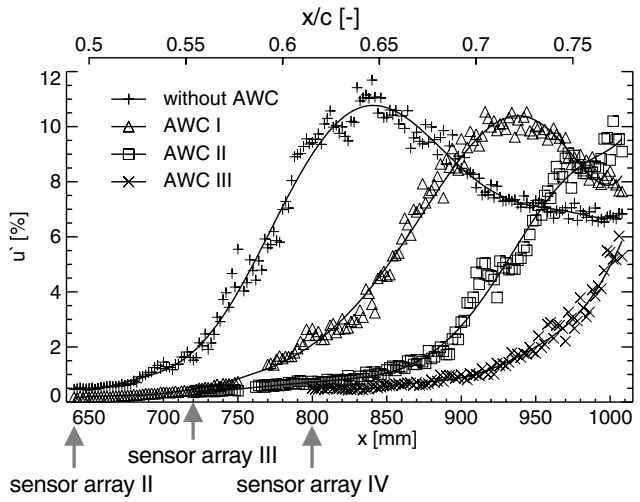

Fig. 18. Streamwise development of u' with subsequently activated control and without control.

control stages are operational. A total TS reduction of approximately 30 dB (≈96%) is achieved if all cascades are activated.

The streamwise amplification of the velocity fluctuation shows the global effect of the multiple stage control as the downstream shifted laminar–turbulent transition. Fig. 18 depicts the amplification curves with and without successively activated cancellation systems. The velocity fluctuation u' was measured by a traversable single hot-wire probe in a constant wall distance of $y = 1.1$ mm downstream of the sensor–actuator systems employed. The u' values were normalized by the freestream velocity. A delay in transition of $\Delta x \approx 90$ mm is obtained when only the first cascade is activated (AWC I). In this case, a slightly decreased amplification rate can be observed. This is caused by the fact that the first system is capable of canceling 2D waves only. The remaining, predominantly three-dimensional disturbances are amplified with a smaller gradient. The total transition shift is increased to $\Delta x \approx 240$ mm ($x/c \approx 18\%$) by operating all control cascades (AWC III). No further change in the amplification rate can be observed, due to the appropriate spanwise resolution of the second and third stage with single systems. The arrangement chosen ensures a uniform attenuation of all instability modes.

6. Conclusion

A sensor–actuator system combined with an adaptive control algorithm was successfully applied to achieve a powerful attenuation of naturally occurring TS instabilities on an unswept wing. Recent investigations have shown the potential of multiple control systems canceling TS instabilities to enhance the delay of the laminar–turbulent transition considerably.

Three-dimensional disturbances were reduced by an appropriate spanwise arrangement of single sensor–actuator systems. The multiple spanwise sensor–actuator system was operated by a multi-channel control algorithm adapting autonomous transfer functions simultaneously. Natural TS instabilities as well as artificially induced 3D disturbances with an oblique angle of up to $\Psi = 16°$ were successfully damped with a reduction in amplitude in excess of 94%.

Further experiments have shown the efficiency of a streamwise repeated control to increase the delay of the transition significantly. Three cascades were applied, with only the first stage being a pure 2D system. The subsequent stages downstream consisted of spanwise arranged single systems to ensure the damping of the remaining three-dimensionally dominated disturbances. The total transition shift amounts to $\Delta x \approx 240$ mm ($x/c \approx 18\%$) if all control cascades are operational.

Acknowledgement

The work on Active Wave Control was financially supported by the German Research Foundation DFG (Deutsche Forschungsgemeinschaft).

References

Baumann, M., Nitsche, W., 1996. Investigation of active control of Tollmien–Schlichting waves on a wing. In: Henkes, R., van Ingen, J. (Eds.), Transitional Boundary Layers in Aeronautics, vol. 46. KNAW, Amsterdam, Netherlands, pp. 89–98.

Baumann, M., Nitsche, W., 1997. Experiments on active control of Tollmien–Schlichting waves on a wing. In: Körner, H., Hilbig, R. (Eds.), New Results in Numerical and Experimental Fluid Mechanics, vol. 60 of NNFM. Vieweg Verlag, Braunschweig, pp. 56–63.

Baumann, M., Sturzebecher, D., Nitsche, W., 2000. Active control of TS-instabilities on an unswept wing. In: Fasel, H., Saric, W. (Eds.), Laminar–Turbulent Transition, IUTAM Symposium Sedona/AZ 1999. Springer-Verlag, pp. 155–160.

Bippes, H., Nitschke-Kowsky, P., 1987. Experimental study of instability modes in a three-dimensional boundary layer. AIAA Paper 87–1336.

Elliott, S., 2001. Signal Processing for Active Control. Signal Processing and its Application. Academic Press, San Diego, London.

Elliott, S., Nelson, P., 1993. Active noise control. IEEE Signal Process. Mag., 12–35.

Gmelin, C., Rist, U., Wagner, S., 2000. DNS of active control of disturbances in a blasius boundary layer. In: Fasel, H., Saric, W. (Eds.), Laminar–Turbulent Transition, IUTAM Symposium Sedona/AZ 1999. Springer-Verlag, pp. 149–154.

Herbert, T., Fan, X., Haritonidis, J., 1996. Laminar flow control with neural networks. ASME Papers FED-Vol. 242, Proceedings of the ASME Fluids Engieering Division, pp. 87–91.

Joslin, R., Nicolaides, R., Erlebacher, G., Hussaini, M., Gunzburger, M., 1995. Active control of boundary layer instabilities: use of sensors and spectral controller. AIAA J. 33 (8), 1521–1523.

Kachanov, Y., 1994. Physical mechanisms of boundary layer transition. Ann. Rev. Fluid Mech. 26, 411–482.

Ladd, D., 1990. Control of natural instability waves on an axisymmetric body. AIAA J. 28 (2), 367–369.

Ladd, D., Hendricks, E., 1988. Active control of 2-D instability waves on an axisymmetric body. Exp. Fluids 6, 69–70.

Liepmann, H., Brown, G., Nosenchuck, D., 1982. Control of laminar instability waves using a new technique. J. Fluid Mech. 118, 187–200.

Milling, R., 1981. Tollmien–Schlichting wave cancellation. Phys. Fluids 24 (5), 979–981.

Oertel Jr., H., Delfs, J., 1996. Strömungsmechanische Instabilitäten. Springer-Verlag, Berlin, Heidelberg, New York.

Pupator, P., Saric, W., 1989. Control of random disturbances in a laminar boundary layer. AIAA Paper 89-1007.

Saric, W., 1992. Laminar–turbulent transition: fundamentals. In: Special Course on Skin Friction Drag Reduction, vol. 786 of AGARD-Report, pp. 4(1–32).

Schlichting, H., Gersten, K., 2000. Boundary Layer Theory, eighth ed. Springer-Verlag, Berlin, Heidelberg, New York.

Smith, S., 1998. The Scientist and Engineer's Guide to Digital Signal Processing, first ed California Technical Publishing, P.O. Box 502407, San Diego, CA 92150-2407.

Snyder, S., 2000. Active Noise Control Primer, Modern Acoustics and Signal Processing. Springer-Verlag, New York.

Sturzebecher, D., 2002. Kaskadierte Sensor-Aktuatorsysteme zur aktiven Dämpfung von natürlichen Tollmien–Schlichting Instabilitäten an einem Tragflügel. In: Fortschritt–Berichte VDI, Reihe 7. VDI Verlag, Düsseldorf, PhD-thesis at the Technical University Berlin.

Sturzebecher, D., Nitsche, W., 2002. Active control of Tollmien–Schlichting instabilities by multi-channel sensor actuator systems. In: Wagner, S., Rist, U., Heinemann, H., Hilbig, R. (Eds.), New Results in Numerical and Experimental Fluid Mechanics III, vol. 77 of NNFM. Springer-Verlag, NY, pp. 375–382.

Sturzebecher, D., Anders, S., Nitsche, W., 2001. The surface hot wire as a means of measuring mean and fluctuating wall shear stresses. Exp. Fluids 31, 294–301.

Thomas, A., 1983. The control of boundary layer transition using a wave-superposition principle. J. Fluid Mech. 137, 233–250.

Wirnitzer, B., Schönig, C., Sepp, W., 1994. Spürnase: Adaptive Filter in der Signalverarbeitung, Teil 1: Funktionsprinzip der Adaption. ELRAD Heft 8, pp. 28–31.